Characterisation of the Glare Properties of Photovoltaic Modules and PV Systems Using a Photographic Camera

Donat Hess[1] (iD) and Christof Bucher[1] (iD)

[1] Bern University of Applied Sciences, Switzerland

*Correspondence: Christof Bucher, christof.bucher@bfh.ch

Abstract. With the increasing prevalence of photovoltaic (PV) installations on north-facing roofs in urban areas, the issue of glare on PV modules is becoming more significant. This paper presents a method for measuring and characterising the intensity and type of glare using a commercially available photo camera. The method utilises the fact that brightness information is inherently contained in a photograph. Due to the strong non-linearity of brightness information in an image, especially when using High Dynamic Range (HDR) functionality, an image needs to be divided into multiple sub-images with clearly defined settings, and the linear range extracted from each of them. The information obtained in this way is then assembled into a new image. The resulting luminance image describes the intensity and shape of glare, forming the basis for calculating the occurrence of glare (times and days of the year) in a simplified manner.

Keywords: Glare Measurement, Reflection, Luminance of Photovoltaic Modules

1. Introduction

PV modules are generally designed to be low in reflection to maximise energy yield. The reflection coefficient is usually less than 10%, significantly lower than that of most other surfaces in built environments [1]. However, unlike other surfaces, reflections on most glasses are directional rather than diffuse.

The reflective properties of standard solar glass lie between those of window glass or a mirror (fully directional, specular reflection) and those of a matt surface, such as a white plastered wall or satinated glass [2]. The partially diffuse reflection of solar glass results in the luminance of the reflection spot being reduced by several orders of magnitude, but it becomes larger in size. In other words, this means that glare (defined here as a reflection that is perceived as disturbing due to its brightness) may be less bright but can be observed over a longer period. This phenomenon of partially directional and partially diffuse reflection is called beam spread.

Previous works have considered beam spread as a constant value in degrees [3, 4]. While this provides a reference for extending the duration of glare, it only applies to nearly perpendicular incidence of light on a PV module. When the sun falls at a shallower angle on a module, as is often the case with glare, the glare spot deforms into an ellipse [2].

Typically, this ellipse appears "narrow and tall": the major axis extends towards the light source (sun), while the minor axis lies perpendicular to it. This results in the beam spread in

reality not having the same effect on extending the calendrical glare (number of days in the year) as on the temporal glare (number of hours in the day).

In [2], this phenomenon is described and approximated with an empirically measured function. The major and minor axes of the glare ellipse are presented as a function of the angle of incidence of the sunlight onto the module plane. The measurements for this were conducted using both a device for determining the Bidirectional Reflectance Distribution Function (BRDF) as well as with a commercially available Digital Single-Lens Reflex (DSLR) camera.

In [5], gonireflectometric measurements were employed to compare various glass surfaces used in photovoltaic (PV) installations and to estimate their glare impact by calculating retinal irradiance. Also [6] uses goniophotometry to assess glare of surfaces. However, the corresponding measuring device is large and expensive and is only used by a few laboratories. It also cannot be used to take measurements outdoors.

The aim of this paper is to find a simple method for measuring and characterizing glare. The method is intended to work using commercially available means without special measuring devices. Different measurement methods are compared with each other. The method of choice is based on a standard DSLR camera but would also work with any other camera as long as aperture, ISO value, opening time and other factors affecting image brightness can be controlled. The basis for creating calibration and measurement software is presented.

1.1 Term Definitions

The relevant definitions used in this document are listed below.

1.1.1 Glare-Free Module

In this paper, a glare-free module is defined based on [2]. A glare-free module is a module whose luminance (brightness) is lower or equal under all relevant angles of incidence of light compared to the luminance of a surface judged as glare-free by an independent third party. The proposed threshold values for defining a glare-free module depend on the incident angle and vary from 30'000 cd/m² for angles between 0° (perpendicular light on a PV module) to 50°, then they are gradually increased to 400'000 cd/m² for incident angles of 80°. For incident angles >80° glare is supposed not to be relevant anymore, as the observer sees both the glaring surface and the sun in a similar direction.

1.1.2 Glare Spot

The glare spot refers to the zone of visible reflection whose luminance exceeds the threshold shown in the definition of "glare-free module". Accordingly, the size of the glare spot depends on the angle. Up to and including 50°, the threshold for the glare spot intensity is 30'000 cd/m², at 60° it is 40'000 cd/m², at 70° it is 100'000 cd/m², and at 80° it is 400'000 cd/m² (**Figure 1**). Alternatively, the glare spot is defined as the area of the specular reflection that has a luminance of over 30'000 cd/m² regardless of the angle of incidence. **Figure 2** shows and illustrates the glare spot for steep and shallow angles of incidence according to both definitions.
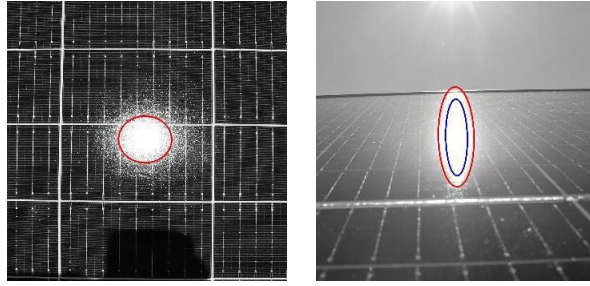
Figure 1. *Size and shape of the glare spot at a 5° angle of incidence (steep incidence, left) and 80° angle of incidence (shallow incidence, right). The red ellipse marks the area with a luminance >30,000 cd/m², while the blue ellipse denotes the area with luminance > 400,000 cd/m². The photo suggests that at a shallow angle of incidence, the entire field of view of the observer is uncomfortably bright.*

2. Measurement of Glare

2.1 Overview of Measurement Methods

To determine the reflection properties of PV modules, four measurement methods and one reference method are introduced (Table 1):

Table 1. *Measurement methods used in this paper*

| Method name	Description
M0_Ref	Reference method. These measurements are done with a calibrated BRDF measurement system provided by SPF, the Institute for Solar Technology of the Eastern Swiss University of Applied Sciences (OST) [8]
M1_MS_in	Measurements done with the calibrated Mavo-Spot, indoor
M2_MS_out	Measurements done with the calibrated Mavo-Spot, outdoor
M3_cam_in	Measurements done with a DSLR camera, indoor. This is the main method under investigation in this paper.
M4_cam_out	Measurements done with a DSLR camera, outdoor. This method was presented in [2] and will not be investigated in detail in this paper.

These methods are applied at the PV laboratory of the Bern University of Applied Sciences (BFH). In all measurement methods, the aperture properties of the modules are characterised by luminance. The individual methods will be presented in more detail in the following subsections. The advantages and disadvantages of the measurement devices and the measurement locations are summarised in Table 2.

Table 2. *Advantages and disadvantages of the measurement devices and the location of the measurement (indoor or outdoor) for characterising the glare properties of PV modules*

Description	Advantages	Disadvantages
Reference method M0_Ref	• Complete BRDF • Enables characterisation of glare shape	• Only a small area of the module is examined • Not applicable in the field
Mavo-Spot	• Measurement device calibrated • Applicable in the field	• Only point measurement possible
DSLR camera	• Cost-effective • Entire module is examined • Allows characterisation of glare shape • Applicable in the field	• Requires tripod • No complete BRDF • Measurement uncertainty cannot be calculated precisely
Outdoor	• Full sunlight spectrum • Correct sun size • Applicable to PV systems	• Weather dependent • High measurement uncertainty
Indoor	• Weather independent • Consistent conditions	• Indoor to outdoor conversion errors

2.2 Overview of Investigated Surfaces

In this paper, five surfaces are examined for their glare properties. The glasses and modules under investigation are depicted in **Figure 2** and described in Table 3.
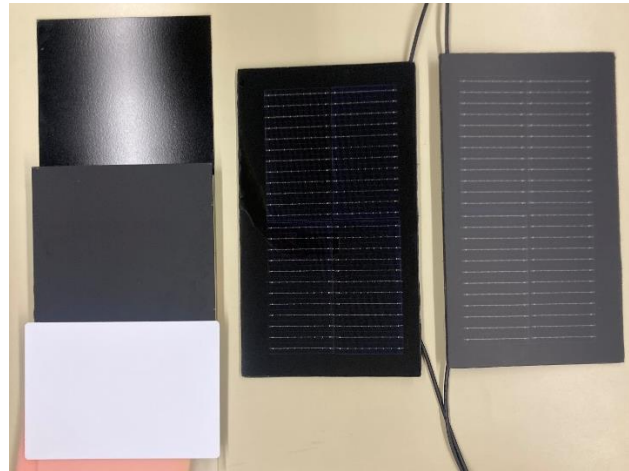
Figure 2. *Investigated surfaces: Standard glass S1_standard (top left), satinated glass S2_satinated (middle left), white reference surface S5_refWhite (bottom left) and mini module with float glass S3_float (middle) and with anti-glare foil S4 foil (right).*

Table 3. Overview of the investigated surfaces with brief descriptions

Surface name	description
S1_standard	**Standard solar glass** is commonly employed in the manufacturing of most photovoltaic modules. It exhibits some degree of beam spread in its reflection. This type of glass is characterized by a relatively smooth surface and high transparency. It is sprayed with black matte spray to be comparable with modules.
S2_satinated	**Satinated glass** features a matte surface that efficiently scatters reflected light. It is specifically employed in Building Integrated Photovoltaics. It is sprayed with black matte spray on the back to be comparable with modules.
S3_float	**Float glass** (mini module from 3S) measures approximately 49.5 cm x 28.5 cm and is coated with float glass. The surface of float glass is completely flat and shows no beam spread.
S4_foil	**Foiled float glass** is mini module with an anti-glare film. For example, it allows for reducing glare on already installed modules in case of glare complaints.
S5_refWhite	The **white reference surface** is a standard white balance card for photography in the size of a A4 paper.

2.3 Reference Method (M0_Ref)

In [8], SPF presents a method for characterising the Bidirectional Reflectance Distribution Function (BRDF) of the luminance of a PV module. In this paper, this method is referred to as M0_Ref. In this setup, a section (15 mm x 20 mm) of the PV module under investigation is positioned in the centre of a non-reflective surface enveloped by a light-absorbing hemisphere. The section of the PV module is illuminated by a beam of light at a specific angle, resulting in the angle-dependent reflection of the beam on the inside of the hemisphere. This reflection is fully captured by a CCD camera via a curved mirror.

2.4 Handheld Luminance Meter Mavo-Spot (M1_MS_in and M2_MS_out)

One way to determine the maximum brightness of a glare spot on a PV module is by using a handheld luminance meter. Such a device is the Mavo Spot 2 USB Luminance Meter, which was utilised in [7] to determine the angle-dependent brightness of glare spots on PV modules. The Mavo-Spot allows for the determination of the mean luminance of a field of view with a 1° diameter. The measuring range extends from 0.01 cd/m² to 99'990 cd/m², which can be expanded to 99'990'000 cd/m² with a screwon grey filter with a factor of 1000 cd/m². However, due to the point measurement (1° diameter) with this device, the identification of the glare shape is not possible. Additionally, identifying the centre of the glare spot requires numerous measurements, which can be distorted by point reflections on busbars.

2.5 Determination of Luminance using Camera and Conversion Software

A method to convert RGB pixel values into luminance values is described in Table 4. However, for simplicity reasons this step is done using the software IQ-Luminance in this paper. Converting pixel values to luminance requires the identification of camera-specific parameters, which are experimentally determined by the company Image Engineering. This calibration is conducted for different aperture settings and exposure times and is only valid for a given ISO value and zoom setting. For accurate determination of luminance, camera sensors must neither be over- nor undersaturated. To assess the range in which luminance images from IQ-Luminance, based on camera captures, provide approximately correct values (deviation <10%), S5_refWhite with known luminance values is photographed with various camera settings using raw image format, and the luminance is determined again using IQ-Luminance. In Table 5, luminance measurements that deviate less than 5% from the Mavo-Spot value are

marked in green, those deviating between 5% and 10% are marked in yellow, and those deviating more than 10% are marked in red. Additionally, each measurement indicates the range in which the RGB values of the photographed object lie. RGB values can range from 0 to 255 counts depending on the stimulation of the camera's red, green, and blue light sensors. It is observed that in most cases where the deviation is greater than 10%, the sensors are either over- or undersaturated (RGB values nearing 0 or 255 counts). An exception is camera settings with an exposure time shorter than (1/1000) s.

Table 4. Conversion method for converting RGB values into luminance values [9]

Step	Description	
1	convert 8 bit RGB image into decimal value: C_{srgb} = C8/255	C8 = {R8, G8, B8}
2	Read out value per colour $C = ((C_{srgb}+0.055)/1.055)^{2.4}$ $C = C_{srgb}/12.92$	if C_{srgb} > 0.03928 if C_{srgb} <= 0.03928
3	Add values of different colours: $L = 0.2126R + 0.7152G + 0.0722B$	where C={R, G, B}

Table 5. Deviation of luminance values determined with iQ-Luminance from those determined with the Mavo-Spot for different camera settings. The minimum and maximum RGB values of the photographed objects are also provided.

Aperture opening / Exposure time (Lumincance Mavo-Spot)	5 cd/m²	100 cd/m²	1'000 cd/m²	3'000 cd/m²	30'000 cd/m²	100'000 cd/m²
F/3.5 (1/30) s	R: 14-22 G: 10-16 B: 4-9	R: 200-216 G: 183-200 B: 133-154	R: 255-255 G: 255-255 B: 255-255	R: 255-255 G: 255-255 B: 255-255		
F/4 (1/60) s	R: 5-10 G: 3-7 B: 0-5	R: 132-150 G: 114-133 B: 74-90	R: 255-255 G: 255-255 B: 255-255		R: 255-255 G: 255-255 B: 255-255	
F/5.6 (1/125) s	R: 0-4 G: 0-2 B: 0-3	R: 26-34 G: 23-28 B: 13-20	R: 172-193 G: 195-213 B: 195-213	R: 210-224 G: 232-244 B: 234-248		
F/8 (1/250) s	R: 0-3 G: 0-1 B: 0-1	R: 5-10 G: 4-7 B: 1-6	R: 54-68 G: 69-79 B: 68-80	R: 147-175 G: 171-198 B: 174-198	R: 242-255 G: 243-255 B: 245-255	R: 255-255 G: 255-255 B: 255-255
F/11 (1/500) s		R: 1-3 G: 0-3 B: 0-4	R: 14-20 G: 18-23 B: 17-24	R: 41-54 G: 52-63 B: 54-64	R: 185-209 G: 210-233 B: 214-237	R: 241-255 G: 242-255 B: 244-255
F/16 (1/1000) s			R: 1-6 G: 3-7 B: 3-7	R: 8-13 G: 11-15 B: 10-17	R: 124-155 G: 146-180 B: 147-182	R: 129-215 G: 154-236 B: 156-241
F/11 (1/2000) s			R: 1-6 G: 3-6 B: 2-7		R: 129-162 G: 153-185 B: 155-188	R: 138-214 G: 162-237 B: 165-240
F/16 (1/4000) s			R: 0-3 G: 0-3 B: 0-4		R: 25-45 G: 33-55 B: 32-57	R: 136-185 G: 158-209 B: 161-211

Legend: Dev. < 5% | Dev. 5%-10% | Dev. > 10%

2.6 Measurement Glare Spot with a Camera (M3_cam_in and M4_cam_out)

To fully capture the luminance of a glare spot using a camera and conversion software, luminance images based on different camera settings need to be combined. Since a glare spot on a PV system can range from values between 10^3 cd/m² (luminance of the module) to over 10^8 cd/m² (centre of the glare spot), a single photo provides information only for calculating the luminance in a portion of the glare spot due to under- and over-saturation of the sensors. In order to reliably determine the luminance across the necessary five decades, the glare spot is photographed with six different camera settings in the method presented below. The resulting luminance images are processed into a composite image. The measurement process is summarised in as a flowchart (**Figure 3**).

To ensure that the six images are captured from a consistent position, a tripod is used along with the continuous shooting mode. The tripod is installed in such a way that the camera photographs the surface from the angle of incidence corresponding to the projector light's angle. To avoid manually selecting camera settings, triple continuous shots are taken with exposure times of 1/2 s, 1/15 s, and 1/125 s, while maintaining a constant aperture of F3.5, ISO 100, and a zoom of 18 mm for indoor measurements. The continuous shooting sequence is then repeated with a grey filter held in front of the camera, which reduces luminance by a factor of 1000. The images generated in this way cover the brightness of the entire glare spot.

The six luminance images are averaged into one image based on RGB values. As a selection criterion for the individual luminance image areas, it was determined that the RGB values of the underlying photo capture must be within the range from 15 to 240. This is intended to reduce the measurement error to below 10%. As shown in Table 2, all values with exposure times longer than (1/2000) s and aperture openings wider than F/16 exhibit deviations smaller than 10% under these conditions.

The RGB values are converted into luminance values using the IQ-Luminance software. This ensures a basic calibration of the transformation. However, RGB values below 15 and above 240 are close to saturation and therefore contribute disproportionately to the measurement uncertainty. Therefore, the luminance values of the six images are combined with a weighting factor w_i of image i which is 1 for an RGB value of 255/2 and decreases linearly to 0 for an RGB value of 15 or 240. The averaging is performed over the logarithm of the luminance of the images so that the RGB weighting is linear with respect to visual perception. Therefore, the formula for calculating the luminance L of the six combined images is:

$$L = \exp\left(\frac{\sum_1^6 w_i \ln(L_i)}{\sum_1^6 w_i}\right) \tag{1}$$

where L_i represents the luminance of image i.

Figure 3. Overview of the process of measuring glare spots on a PV system using a camera.

2.7 Indoor Measurement (M1_MS_in and M3_cam_in)

Glare on PV modules can also be measured indoors using a uniformly distributed light source. To ensure measurements are not weather-dependent, both camera-based measurements and Mavo-Spot measurements were conducted indoors (M1_MS_in and M3_cam_in). A projector was used as the uniform light source, with built-in polarisation filters removed. The PV modules

were illuminated by the projector in a darkened room (aside from the projector light, luminance everywhere was below 10 cd/m²) from a distance of 19 meters. To compare the measurement results with reflections from other light sources (e.g., the sun), the obtained luminance values need to be scaled.

The scaling factor chosen was the ratio of the luminance of S5_refWhite illuminated perpendicularly by a reference light source to the luminance of S5_refWhite illuminated by the projector. To ensure the comparability of all measurements, all indoor as well as outdoor measurements were scaled to the intensity of the light source of M0_Ref.

3. Validation of Measurement Methods

The measurement methods presented in Table 1 are compared in this chapter. The luminance of four different surfaces is determined under the incidence angles of 5°, 10°, 20°, 30°, 40°, 50°, 60°, 70°, and 80° using the three measurement methods and compared to each other. The five surfaces presented in Table 3 are used for comparison.

For scaling the indoor measurements to outdoor measurements, the angle-dependent luminance of the surface of the S3_float (highly reflective) and the S5_refWhite were determined indoors and outdoors using the Mavo-Spot.

To make the luminance measurements taken with the camera comparable to those of the reference method M0_Ref, similar areas must be compared. While M0_Ref captures reflection in all directions, the camera captures reflection only in an area around the reflection angle corresponding to the incident angle. However, with matt surfaces like S2_satinated or S5_refWhite, the incidence angle does not match the angle of reflection, and the strongest reflection might be outside the photographed area. In order to be able to compare the two measurement methods, areas outside the visible glare zone were excluded from the image processing. In the following subsections, the results of the different measurement methods are compared with each other. **Figure 4** provides an overview of all the measured luminances.
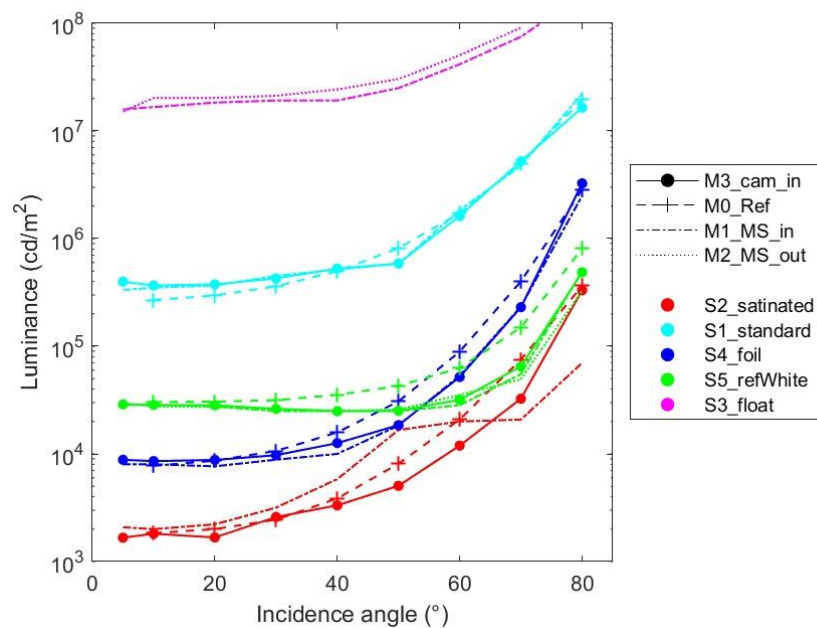

Figure 4. *Angle-dependent luminance of five different surfaces and four measurement methods.*

3.1 Comparison of Mavo-Spot and Camera-Based Measurements

The deviations between the Mavo-Spot indoor measurements and the M3_cam_in are shown in **Figure 5**. The deviations for S1_standard, the S4_foil and S5_refWhite are all below 20%, except for S1_standard at an angle of incidence of 80° (35% deviation), while S2_sainated exhibits deviations of more than 20% at most angles. These deviations will be discussed in the following paragraph.
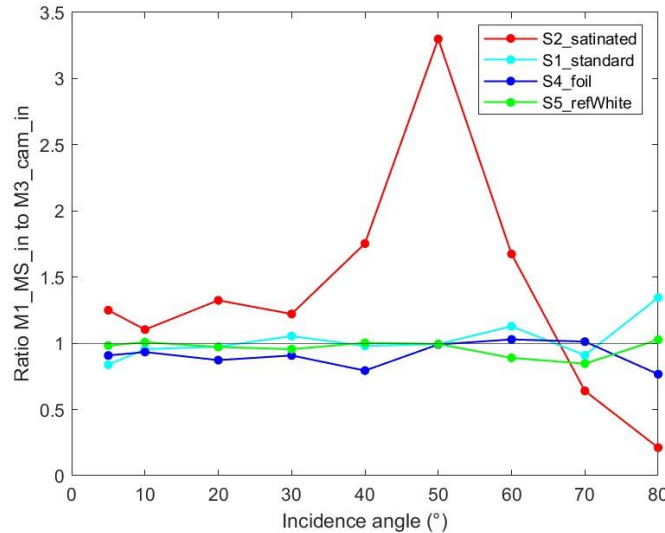
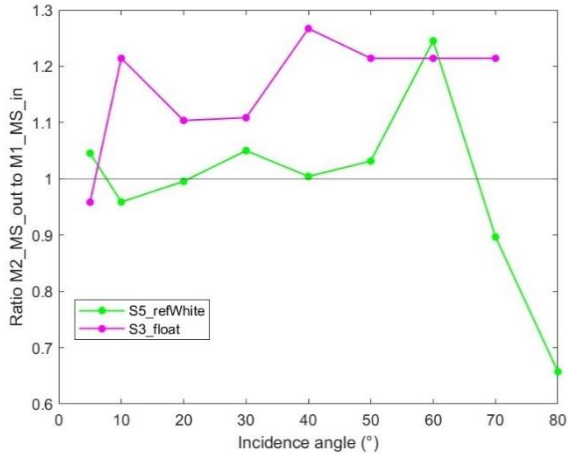*Figure 5. Ratio of luminance M1_MS_in to M3_cam_in as a function of the incidence angle.*

The deviations observed for S2_satinated can be attributed to the fact that the Mavo-Spot did not measure the same reflection area as the camera. For S2_satinated, the incident angle and the reflection angle are not the same. For example, at an incident angle of $\theta = 50°$ the maximum reflection is observed at a reflection angle of roughly 80°. This angle is not anymore within the observed area of the camera.

## 3.2 Validation of the Conversion from Indoor to Outdoor Measurements

As indoor measurements are done using a light source which creates luminance values several orders of magnitude below the luminance values in direct sunlight, the results must be converted to equivalent expected outdoor values. The verification is done using S4_refWhite and S3_float. The deviations between indoor and outdoor luminance are consistently below 35% (**Figure 6**).

3.3 Comparison of M3_cam_in and M0_Ref

At small incidence angles (< 30°), the luminances of M0_Ref and M3_cam_in agree with a maximum relative difference of 27% (**Figure 7**). However, deviations increase at larger incdence angles. For incidence angles from 50° to 70°, deviations of 50% to 130% are observed for the matt glasses (S2_satinated, S4_foil, and S5_refWhite). At 80° luminances converge again.

Figure 6. *Ratio of M2_MS_out to M1_MS_in. The highly reflective S3_float and the matt S5_refWhite are being investigated.*
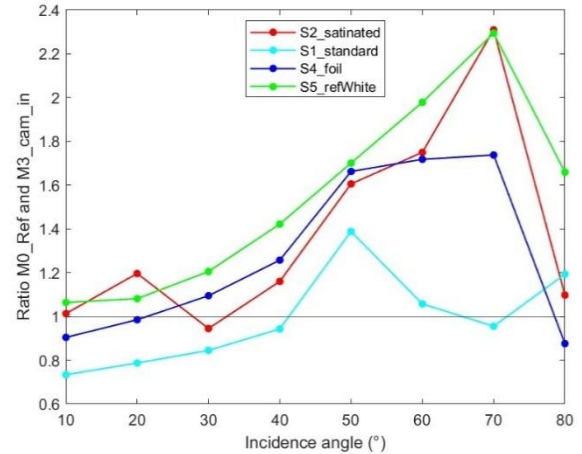
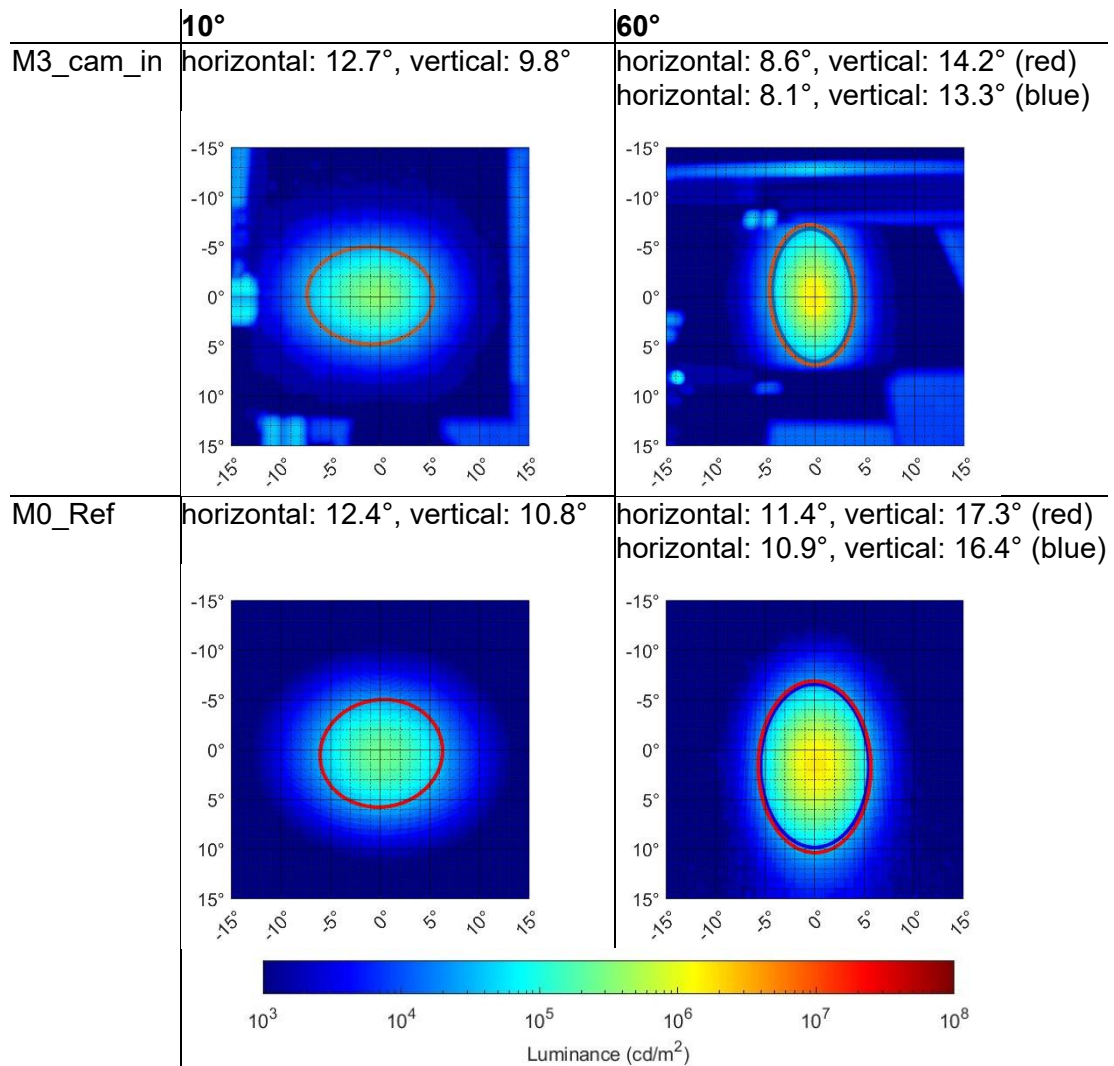**Figure 7.** *Ratio of luminances measured with M0_Ref and M3_cam_in.*

3.4 Characterisation of the Glare using M0_Ref and M3_cam_in

As shown in **Figure 1** and **Figure 9** the shape of glare is typically elliptical. The shape and size of this ellipse can be described by a horizontal and a vertical axis. In **Figure 8**, the incident angle dependent axes of the elliptical glare on S1_standard are shown. They are measured with the reference and M3_cam_in. From 60° onwards, both the angle independent glare definition with constant luminance of > 30'000 cd/m² (lower branch) and the angle-dependent definition where glare has a luminance > 40'000 cd/m² at 60° and > 100'000 cd/m² at 70° (higher branch) are given. For the angle of 80°, the glare is not fully within the measurement range of most methods and could therefore not be characterised. This is also the case for M3_cam_in at 70° in the case of the vertical axis. For illustration, the luminance images of the two methods for the incidence angles of 10° and 60° are shown in **Figure 9**. In M3_cam_in luminance images, the origin is given by the brightest point of the glare, while for M0_Ref, the origin corresponds to the angle of incidence. Thus, the deviation between the centre of the glare spot and the coordinate origin indicates for M0_Refthe average difference between the angle of incidence and the angle of reflection.

Both in M3_cam_in and M0_Ref, it is observed that at small incidence angles, the horizontal axis is larger than the vertical axis. At an irradiation angle of 10°, the horizontal axes in M3_cam_in and M0_Ref are 12.7° and 12.4°, respectively, while the vertical axes are 9.8° and 10.8°. With increasing the incidence angle, the horizontal axis decreases, and the vertical axis increases. At an incidence angle of 60°, the horizontal axis sizes are decreased to 8.6° and 11.4°, while the vertical axis sizes are grown to 14.2° and 17.3°. It is noted that in M0_Ref, the horizontal axis decreases more rapidly, and the vertical axis increases more rapidly than in M3_cam_in. Up to an angle of 50°, this observation could be explained by the fact that the maximum luminance in M0_Ref increases more rapidly with increasing incidence angle than that of M3_cam_in. Additionally, one explanation for the fact that the ellipse of M0_Ref mostly exhibits larger values than that of M3_cam_in could be different sizes of the light sources used.
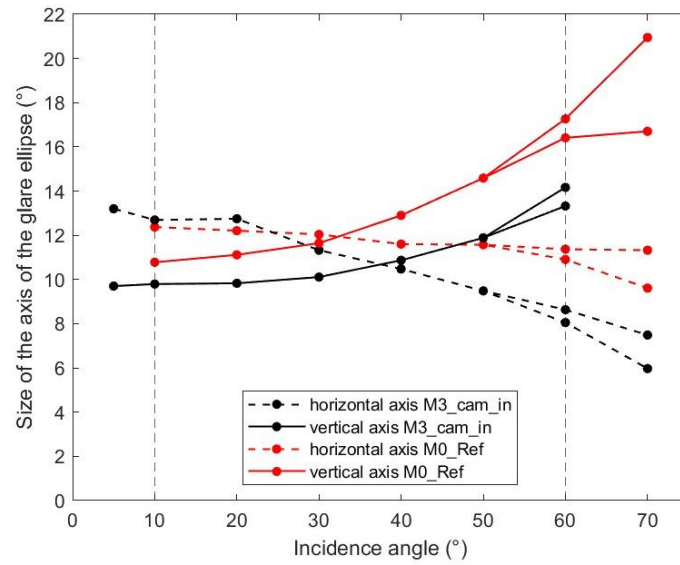
Figure 8. *Horizontal and vertical axis sizes of the elliptical glare spot on S1_standard. From 60° on-wards, both the glare definition with constant luminance of > 30'000 cd/m² (lower branch) and the angle-dependent definition are provided.*

	10°	60°
M3_cam_in	horizontal: 12.7°, vertical: 9.8°	horizontal: 8.6°, vertical: 14.2° (red) horizontal: 8.1°, vertical: 13.3° (blue)
M0_Ref	horizontal: 12.4°, vertical: 10.8°	horizontal: 11.4°, vertical: 17.3° (red) horizontal: 10.9°, vertical: 16.4° (blue)

Figure 9. *Luminance images. The red ellipse denotes the glare spot according to the definition with angle-independent luminance (< 30'000 cd/m²), and the blue ellipse denotes the glare spot according to the angle-dependent glare definition (< 40'000 cd/m² at 60°).*

4. Conclusion and Outlook

The results show that it is possible to measure the luminance of glare from an indoor PV system using a photo camera. Although measurement deviations of up to 35% between the methods in this work and up to 130% with the reference method M0_Ref were found, this may still be acceptable for some applications, as the expected results vary over five orders of magnitude and are presented on a logarithmic scale.

In future, the measurement method is to be automated developing a new software. The differences between the measurements are to be further analysed and the method improved, e.g. using better calibration techniques or more controllable indoor light sources. In addition, the software/process is to be made sufficiently barrier-free for non-specialists.

Data availability statement

The data for this project is not publicly available.

Author contributions

Donat Hess: conceptualization, data curation, formal analysis, validation, visualization, writing – original draft. **Christof Bucher**: conceptualization, formal analysis, funding acquisition, methodology, project administration, resources, supervision, validation, writing – review & editing.

Competing interests

The authors declare that they have no competing interests.

References

[1] Sunpower Corporation, "Photovoltaic Systems: Lower Levels of Glare and Reflectance vs. Surrounding Environment: Possible Glare & Reflectance in PV Systems," Sunpower, Possible Glare & Reflectance in PV Systems, 2019.

[2] C. Bucher, A. Bohren, D. Hess, S. El Hassani, and M. Hügi, "Two-Dimensional Representation of the Bidirectinal Reflectance Distribution Function of Photovoltaic Modules," EU PVSEC, vol. 2023.

[3] Sandia National Laboratories, "Solar Glare and Flux Analysis Tools," [Online]. Available: https://www.sandia.gov/glare-tools/

[4] Kanton Bern, "Blendtool v1.2.0," [Online]. Available: https://www.blendtool.ch/

[5] M. Babin, S. Thorsteinsson, M. L. Jakobsen and S. V. Spataru, "Glare Potential Evaluation of Structured PV Glass Based on Gonioreflectometry," in IEEE Journal of Photovoltaics, vol. 12, no. 6, pp. 1314-1318, Nov. 2022, doi: 10.1109/JPHOTOV.2022.3189779

[6] Noback, Andreas; Grobe, Lars Oliver & Wittkopf, Stephen, Comparing BSDF data from a real and a virtual goniophotometer. 15th International Radiance Workshop, Padua, 2016. Available at https://www.radiance-online.org/community/workshops/2016-padua/presentations/301-Noback-ComparisonOfVirtualGoniophotometer.pdf.

[7] C. Bucher, P. Wüthrich, S. Danaci, and J. Wandel, "Glare Hazard Analysis of Novel BIPV Module Technologies," in Proceedings of the ISES Solar World Congress 2021, Virtual, 2021, pp. 1–9.

[8] F. Ruesch, A. Bohren, M. Battaglia, and S. Brunold, "Quantification of Glare from Reflected Sunlight of Solar Installations," Energy Procedia, vol. 91, pp. 997–1004, 2016, doi: 10.1016/j.egypro.2016.06.267.

[9] Relative luminance, Wiki page edited by participants of the WCAG Working Group, https://www.w3.org/WAI/GL/wiki/Relative_luminance, accessed 2024-05-17.